LA-UR--91-1487

DE91 013653

Los Alamos National Laboratory is operated by the University of California for the United States Department of Energy under contract W-7405-ENG-36

TITLE METASTABLE PHASE EQUILBRIA IN Co-DEPOSITED $Ni_{1-x}Zr_x$THIN FILMS

AUTHOR(S) J. B. Rubin
R. B. Schwarz

SUBMITTED TO To be published in Materials Research /society Symposia Proceedings, Spring 1991, Anaheim, CA

DISCLAIMER

This report was prepared as an account of work sponsored by an agency of the United States Government. Neither the United States Government nor any agency thereof, nor any of their employees, makes any warranty, express or implied, or assumes any legal liability or responsibility for the accuracy, completeness, or usefulness of any information, apparatus, product, or process disclosed, or represents that its use would not infringe privately owned rights. Reference herein to any specific commercial product, process, or service by trade name, trademark, manufacturer, or otherwise does not necessarily constitute or imply its endorsement, recommendation, or favoring by the United States Government or any agency thereof. The views and opinions of authors expressed herein do not necessarily state or reflect those of the United States Government or any agency thereof.

By acceptance of this article, the publisher recognizes that the U.S. Government retains a nonexclusive, royalty-free license to publish or reproduce the published form of this contribution, or to allow others to do so, for U.S. Government purposes.

The Los Alamos National Laboratory requests that the publisher identify this article as work performed under the auspices of the U.S. Department of Energy.

Los Alamos National Laboratory
Los Alamos, New Mexico 87545

DISTRIBUTION OF THIS DOCUMENT IS UNLIMITED

MASTER

METASTABLE PHASE EQUILIBRIA IN CO-DEPOSITED $Ni_{1-x}Zr_x$ THIN FILMS

J. B. RUBIN and R. B. SCHWARZ

Center for Materials Science and MST-7, Los Alamos National Laboratory, MS K765, Los Alamos, NM 87545

ABSTRACT

We determine the glass forming range (GFR) of co-deposited $Ni_{1-x}Zr_x$ ($0 < x < 1$) thin films by measuring their electrical resistance during in situ constant-heating-rate anneals. The measured GFR is continuous for $0.10 < x < 0.87$. We calculate the GFR of Ni-Zr melts as a function of composition and cooling rate using homogeneous nucleation theory and a published CALPHAD-type thermodynamic modeling of the equilibrium phase diagram. Assuming that the main competition to the retention of the amorphous structure during the cooling of the liquid comes from the partitionless crystallization of the terminal solid solutions, we calculate that for $dT/dt = 10^{12}$ K s^{-1}, the GFR extends to $x = 0.05$ and $x = 0.96$. Better agreement with the measured values is obtained assuming a lower 'effective' cooling rate during the condensation of the films.

INTRODUCTION

The formation of amorphous alloys by rapid solidification techniques requires that crystallization be suppressed during the undercooling of the liquid from its melting temperature, T_m, to the glass transition temperature, T_g. The GFR, or range of compositions over which this undercooling is possible, is determined by a combination of kinetic and thermodynamic factors. For alloys between an early- and a late-transition metal and for conventional quenching methods such as melt-spinning, where the cooling rates are on the order of 10^7 K s^{-1}, the GFR is usually discontinuous, being composed of distinct composition ranges centered near deep eutectics. As the cooling rate is increased, however, these individual composition ranges widen and, for extremely high cooling rates, may overlap to include all intermediate compositions, excluding only the terminal solution regions [1]. The formation of metallic films by condensation from the vapor phase represents an extreme case of rapid quenching, with an effective cooling rate on the order of 10^{12} K s^{-1}. It is expected, therefore, that the GFR for thin films of $Ni_{1-x}Zr_x$ produced by co-evaporation will be continuous over a wide region $x_1 < x < x_2$, bounded by narrow regions of crystalline solid solutions for $0 < x_1$ and $x_2 < x < 1$.

In the present work we investigate the GFR of $Ni_{1-x}Zr_x$ ($0 < x < 1$) thin films prepared by the simultaneous condensation of nickel and zirconium vapors in ultra-high vacuum. We use in-situ electrical resistance measurements during constant heating-rate annealing to detect amorphous → crystalline transformations in the as-deposited films. This data is used to deduce the GFR. We also calculate the GFR by a model to be described in the next section.

Calculation of the GFR

Theoretical modeling of the GFR is important for understanding the basic mechanism for glass formation, and continues to be an area of active research. The basic ideas behind the calculations of the GFR are explained with the help of Figure 1 which shows the binary composition-temperature diagram for a hypothetical A-B alloy. The equilibrium phases are the terminal solutions α and β, the congruent-melting compound γ, and the liquid λ. Also shown are the four T_o curves, defined as the composition-temperature loci at which the free energy of the liquid equals that of the solid phase of the same composition. Therefore, below each T_o curve there exists a thermodynamic driving force for partitionless crystallization. The importance of the T_o curves derives from the observation that under conditions of rapid cooling, partitionless solidification is almost always kinetically favored over solidification involving solute partitioning. Thus, at those compositions where partitionless crystallization can be avoided while the melt is cooled to below T_g, it should be possible to kinetically trap the alloy in the glassy (amorphous) state. Figure 1 also shows an assumed, composition-invariant T_g (dotted line). The T_o criterion predicts that the GFR for our hypothetical binary alloy will consist of the two narrow regions which solidify into the λ phase, as shown at the bottom of the figure. At all other compositions the undercooled liquid crystallizes partitionlessly into either α, β, or γ.

The prediction of glass formation based on T_o curves, however, does not consider kinetics; it assumes that partitionless crystallization occurs instantaneously once it is thermodynamically favored. In practice, a finite undercooling is required to produce an observable nucleation rate and thus the GFR must necessarily depend on the cooling rate. To include the kinetics of solidification in the calculations of the GFR, several authors [2,3] have used isothermal transformation kinetics to calculate Time-Temperature-Transformation (TTT) curves or Continuous-Cooling-Transformation (CCT) curves [4]. Nash and Schwarz [5] have extended the method by combining homogeneous nucleation theory [6] with a CALPHAD modeling of the binary phase diagram to derive CCT curves for NiTi alloys as a function of cooling rate, dT/dt, and alloy composition, x. The results are used to calculate the temperature T '(x,dT/dt) for the formation of a volume fraction ς of crystalline material during cooling at the constant rate dT/dt. Finally, defining a critical value of ς below which the solid can be defined as amorphous, they determined the GFR for rapidly solidified Ni-Ti melts by the intersection of the T ' curves with T_g. The GFR found by this T ' criterion is wider than that predicted from purely thermodynamic arguments.

Figure 2 shows the T_o curves (dashed lines) and T ' curves (solid lines) for terminal solutions of Ni-Zr alloys. These were computed from a thermodynamic modeling of the equilibrium phase diagram. The expressions for the excess free energy of mixing for the liquid, FCC, and BCC phases are given by Saunders [7], while the lattice stabilities are taken from Kaufman and Bernstein [8]. The glass transition temperature T_g is approximated by the crystallization temperature T_x, which is plotted based on literature values.[9,10,11,12,13] The compositions of congruent-melting and high-temperature peritectic compounds for this system are shown by vertical dotted lines. The equilibrium melting- or decomposition- temperature for each compound is indicated by the filled square at the top of the dotted line. Extrapolating a curve drawn through the T_g values (dash-dot line) to intersect the two T ' curves for a cooling rate of

10^{12} K/s gives a GFR which extends from $0.05 < x < 0.96$.

EXPERIMENTAL

$Ni_{1-x}Zr_x$ films were produced by co-evaporation from two electron-beam sources in a UHV system at deposition pressures below $5x10^{-8}$ torr. Each source was controlled by a thickness-rate monitor, enabling us to control the alloy composition during deposition. The alloy deposition rates varied from 0.3 nm s^{-1} for the Ni-rich films, to 1.0 nm s^{-1} for Zr-rich compositions. All films had a total thickness of 400 nm. The depositions were made onto alumina substrata which were polished with 0.25 μm diamond paste. Embedded in these substrata were calibrated platinum thin-film resistors which were used both to heat the substrata and to measure the film temperature. The experimental design and measurement circuit are described in the previous paper of this symposium [14]. Following deposition, the films were annealed in-situ at a rate of 10 K min^{-1} at pressures below 10^{-10} torr. During the anneals, the resistance of the films was measured by an AC four-point probe method. Afterwards, the films were removed from the vacuum chamber and the compositions and thickness determined by Rutherford Backscattering Spectrometry (RBS).

RESULTS

The room-temperature resistivities as a function of alloy composition are shown in Fig. 3. The data fall into three groups, identified by the dashed lines A to B, C to D, and E to F. Samples belonging to each of these regions show distinct features in their resistance vs. temperature annealing curves. As an example, we show in Fig. 4 the normalized resistivity versus temperature curve for a sample of approximately equiatomic composition. Initially, the resistivity decreases linearly with temperature, a to b, which is characteristic of an amorphous structure. Crystallization occurs at about 400°C, c to d, resulting in an abrupt drop in resistivity. This is followed by a second small drop in resistivity at about 495°C. At d, the film is fully crystalline, and further temperature cycling, d ⟷ e, gives a reproducible resistance vs. temperature curve of positive slope.

Annealing curves for compositions $0 < x < 0.1$ are shown in Fig. 5. For clarity, only the heating portions of the curves are shown. Those films containing less than 5 at. % Zr show a positive temperature coefficient of resistivity [(1/R)(dR/dT)], indicating that their structure is largely crystalline. The value of [(1/R)(dR/dT)] decreases for increasing Zr content, and a clear change occurs between the curves labeled B and C. The latter sample shows, for T < 400°C, a temperature-independent resistivity; this is followed by a resistivity drop at about 410°C, which we associate with the crystallization of the amorphous phase (see Fig. 4). This drop is absent in curve B, indicating that this film was crystalline in the as-deposited condition. From this we deduce that the terminal (metastable) solubility of Zr in Ni in co-deposited Ni_xZr_{1-x} films is approximately 8 at.%. A similar analysis of Zr-rich films gives a terminal (metastable) solubility of Ni in Zr to be ≈ 6 at. %.

A more accurate determination of the metastable terminal solubilities is made in Fig. 6, where we plot the resistivity drop accompanying crystallization as a function of

resistivity drop should be proportional to the amount of amorphous phase present. The curves labeled B and C in Fig. 5 are similarly marked as points B and C in Fig. 6 for comparison. Dashed lines are drawn through those points leading to an intersection with $\Delta\rho/\rho = 0$. This Figure identifies five composition regions. For $0 < x < 0.04$ and $0.97 < x < 1$, the as-deposited films are crystalline. For $0.10 < x < 0.87$ the films are single-phase amorphous. The two narrow regions $0.04 < x < 0.10$ and $0.87 < x < 0.97$ represent transition regions where the films most likely contain both crystalline and amorphous phases. This coexistence of phases may reflect local compositional fluctuations.

DISCUSSION

Figure 2 shows that solidification kinetics play an important role in determining the GFR of amorphous alloys. The gap in the published T_g data in the composition range $0.1 < x < 0.3$ can be understood in terms of the competition between the liquid and the high-melting point compounds in this region, especially Ni_7Zr_2, which melts congruently. There is evidence that the structure of a liquid just above a congruently-melting compound shows a similar SRO to that of the crystal [15]. As a result, the formation of this crystalline phase would be difficult to suppress during rapid cooling. This kinetic competition would also be responsible for the difficulty in preparing amorphous alloys near the equiatomic composition because of the presence of NiZr, which also melts congruently. This argument would predict, however, that rapid quenching of a liquid of composition $x = 0.67$ would result in the partitionless crystallization of $NiZr_2$, but this is not observed.

Each crystalline phase has associated with it a T_o curve and a two T ' curves similar to those shown for the terminal solutions. The inability to produce amorphous alloys near $x = 0.2$ indicates that the T ' curves for cooling rates achieved in liquid quenching experiments lie above T_g. For the case of $NiZr_2$, it may be that at these cooling rates the T ' curves are depressed to below T_g, allowing for easy glass formation. Work is in progress to calculate the T ' curves for the crystalline phases.

A comparison of the calculation (Figure 2) with experiment (Figure 6) allows us to estimate an 'effective' cooling rate for the formation of amorphous Ni-Zr thin films by co-deposition in vacuum. Extrapolating the T_g values to intersect the T ' curves for a cooling rate of 10^{12} K s^{-1} gives a GFR of $0.05 < x < 0.96$, while for $dT/dt = 10^8$ K s^{-1}, the predicted GFR is $0.08 < x < 0.92$. The experiments give a range of $0.10 < x < 0.87$. Better aggrement would require assuming an 'effective' cooling rate lower than 10^8 K s^{-1}, which is unrealistic. It is thus clear that the GFR predicted by our model overestimates the actual composition range for glass formation. We discuss next possible reasons for the discrepancy.

The volume fraction of crystal, ς, used to define the GFR, is calculated by integrating the homogeneous nucleation rate equation [4,5],

$$I_h = A \cdot \exp(-K\,\sigma^3 / \Delta G^2)\,. \qquad (1)$$

The calculated GFR is therefore quite sensitive to the values chosen for the free energy difference between the liquid and crystal, ΔG, and the interfacial free energy, σ.

[illegible] in the assessed equilibrium phase diagram, particularly in the position of the liquidus lines. Any such errors would be magnified by the large temperature range over which the thermodynamic modeling of these phases must be extrapolated. Another possible source of error may lie in our estimate of σ for Ni-Zr alloys. These are calculated by a simple weighted average of the σ values for the pure elements, which in turnm are determined by [16]

$$\sigma = 0.45\ \Delta H_f N^{-1/3} V^{-2/3}, \qquad (2)$$

where ΔH_f is the molar enthalpy of fusion, N is Avogadro's number, and V is the molar volume of the liquid. The value for σ of an alloy was assumed to be independent of temperature.

Existing experimental assessments of the Ni-Zr system [17] permit an adequate modeling of equilibrium phases, but the reliability of these models in providing thermodynamic data far into metastable regions must be viewed with caution [18]. Our experimental results, along with similar studies of other systems, could provide a basis for improving modeling techniques. For σ, a more realistic estimate would incorporate a compositional and temperature dependence based on thermodynamic data, but few empirical studies have been made, and the problem would remain of determining non-equilibrium values.

REFERENCES

1. Lin and F. Spaepen, *Acta Metall.* 34, 1367 (1986).
2. D. R. Uhlman, *J. non-cryst. Solids* 7, 337 (1972).
3. L. E. Tanner and R. Ray, *Acta metall.* 27, 1727 (1979).
4. D. G. Morris, *Acta metall.* 31, 1479 (1983).
5. P. Nash and R.B. Schwarz, *Acta Metall.* 36, 3047 (1988).
6. J. H. Hollomon and D. Turnbull, in *Prog. Metall. Phys.*, Vol. 4 (Interscience, New York, 1953). p. 333.
7. N. Saunders, CALPHAD 9, 297 (1986).
8. L. Kaufman and H. Bernstein, *Computer Calculation of Phase Diagrams*, (Academic Press, New York, 1970).
9. Y. D. Dong, G. Gregan, and M. G. Scott, *J. Non-Cryst. Solids* 43, 403 (1981).
10. K. H. J. Buschow, B. H. Verbeek, and A. G. Dirks, *J. Phys. D: Appl. Phys.* 14, 1087 (1981).
11. K. Jansson and M. Nygren, *Mat. Sci. Eng.* 97, 373 (1988).
12. Z. Altounian, T. Guo-hua, and J. O. Strom-Olsen, *J. Appl. Phys.* 54, 3111 (1983).
13. K. H. J. Buschow, *J. Phys. F: Met. Phys.* 14, 593 (1984).
14. R. B. Schwarz and J. B. Rubin, paper in this symposium.
15. B. Predel, in *Calculation of Phase Diagrams and Thermochemistry of Alloy Phases*, eds. Y. A. Chang and J. Smith (TMS-AIME, Metals Park, Ohio, 1980), p. 72.
16. D. Turnbull, *J. Appl. Phys.* 21, 1022 (1950).
17. M. E. Kirkpatrick and W. L. Larsen, *Trans. ASM* 54, 580 (1961).
18. R. B. Schwarz, P. Nash, and D. Turnbull, *J. Mater. Res.* 2, 456 (1987).

ACKNOWLEDGEMENTS

We thank the Los Alamos Ion Beam Materials Laboratory for assistance in the characterization of the films by Rutherford backscattering. This work was supported by the U.S. Department of Energy, Office of Basic Energy Sciences, and by Laboratory Directed Research and Development funds.

FIGURES

Fig. 1. Temperature vs. composition diagram for a hypothetical metallic A-B binary system.

Fig. 2. Calculated T_0 curves for the terminal solutions (dashed) and T ' curves at cooling rates of 10^8, 10^{10} and 10^{12} K s^{-1} (solid). The melting- or decomposition-temperatures of the high-temperature intermetallic compounds are shown by filled squares. Measured crystallization temperatures for melt-quenched $Ni_{1-x}Zr_x$ alloys are shown as filled circles.

Fig. 3. Electrical resistivity for co-deposited $Ni_{1-x}Zr_x$ films. The dashed lines A to B, C to D, and E to F divide the data the Ni-rich crystalline terminal solution, single-phase amorphous alloy, and Zr-rich crystalline terminal solution, respectively. The (+) are data for melt-spun ribbons from Ref. [12].

Fig. 4. Electrical resistivity vs temperature curve for a 400-nm thick amorphous $Ni_{39}Zr_{61}$ film annealed at 10 K min^{-1}.

Fig. 5. Resistivity vs temperature curves for co-deposited $Ni_{1-x}Zr_x$ films. A drop in resistivity due to crystallization is seen for $x \geq 0.1$.

Fig. 6. Change in electrical resistivity caused by crystallization of $Ni_{1-x}Zr_x$ films as a function of composition. Points B, C, D, and E correspond to those in Fig. 3. The intersection of the dashed lines with $\Delta\rho/\rho$ gives the limits of the two metastable terminal solutions.

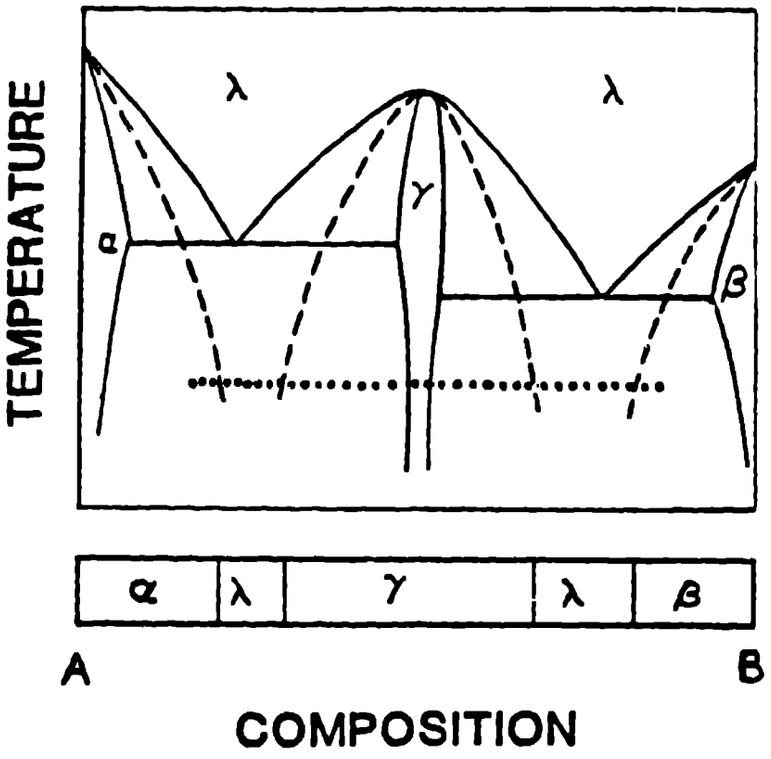

Fig. 1

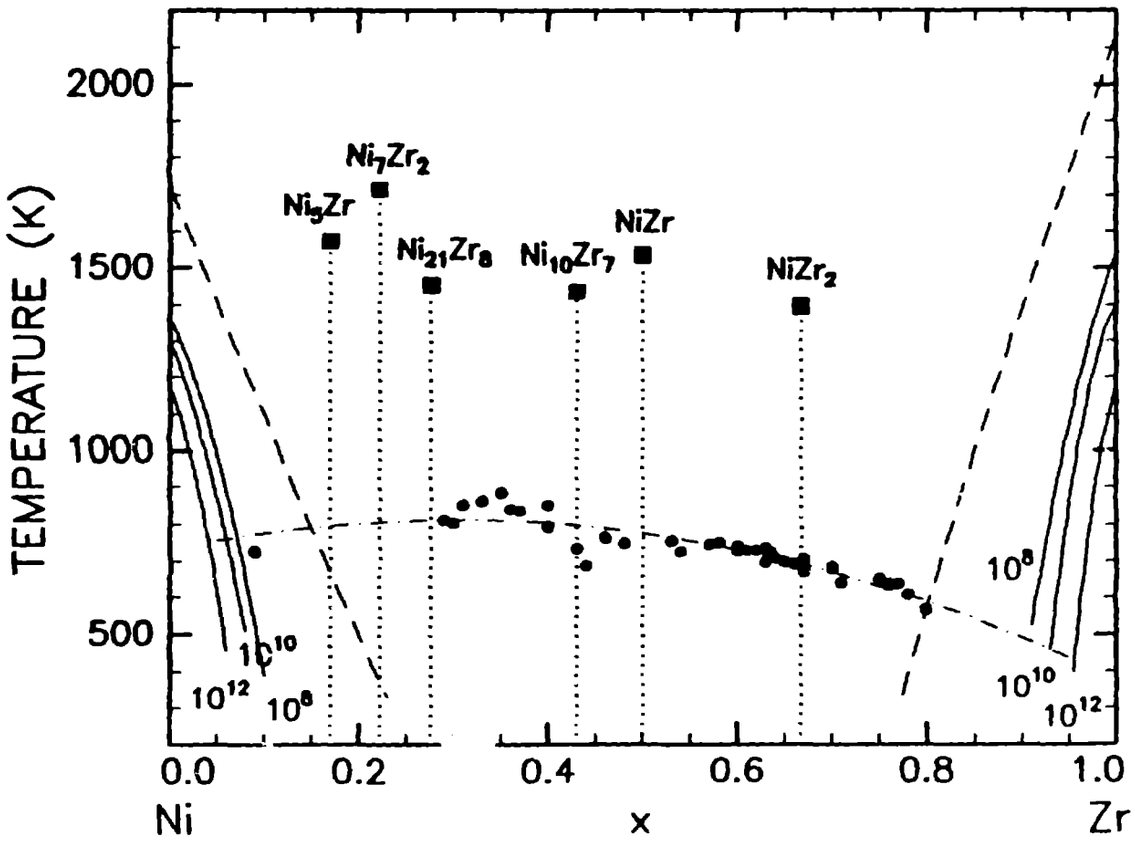
TEMPERATURE (K)
2000
1500
1000
500
Ni_7Zr_2
Ni_5Zr
$Ni_{21}Zr_8$
$Ni_{10}Zr_7$
NiZr
$NiZr_2$
10^{12}
10^{10}
10^8
10^8
10^{10}
10^{12}
0.0
0.2
0.4
0.6
0.8
1.0
Ni
x
Zr

Fig. 2-

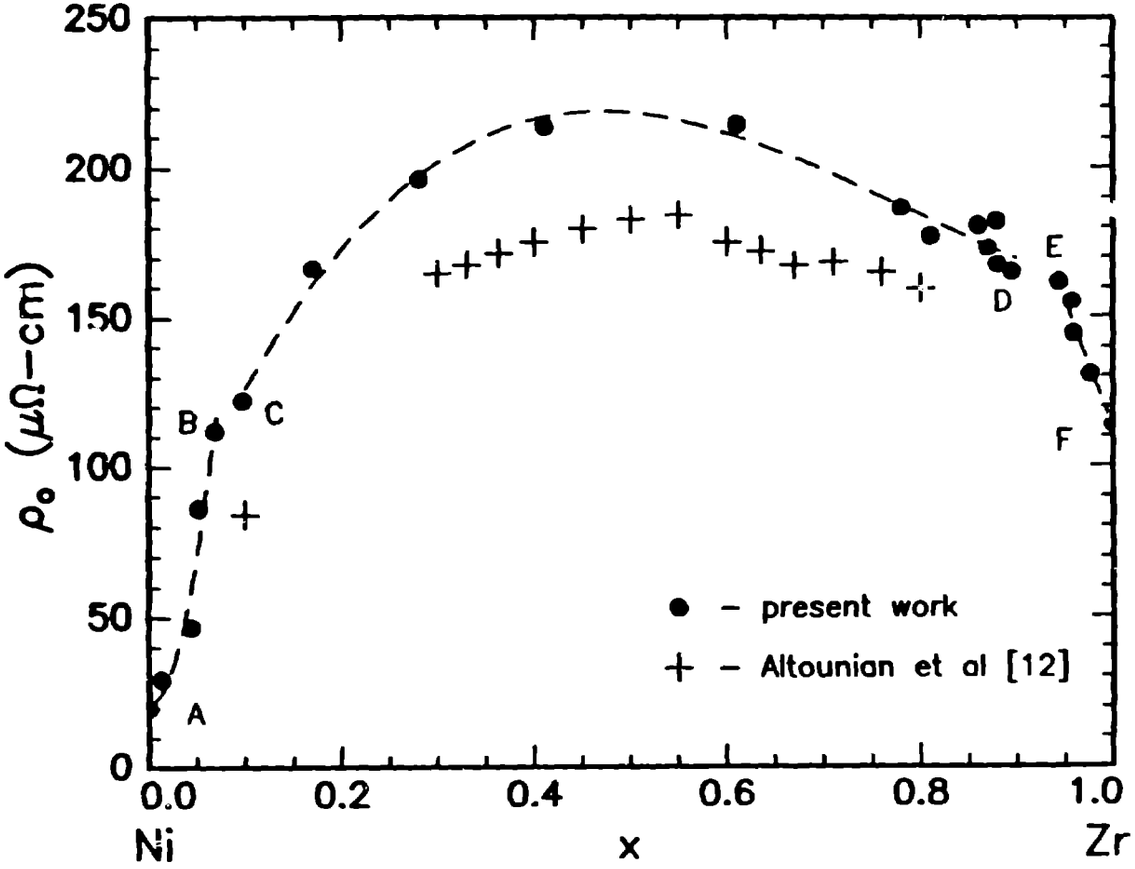
250
200
150
100
50
0
ρ_o ($\mu\Omega$-cm)
A
B
C
D
E
F
● – present work
+ – Altounian et al [12]
0.0
0.2
0.4
0.6
0.8
1.0
Ni
x
Zr

Fig. 3

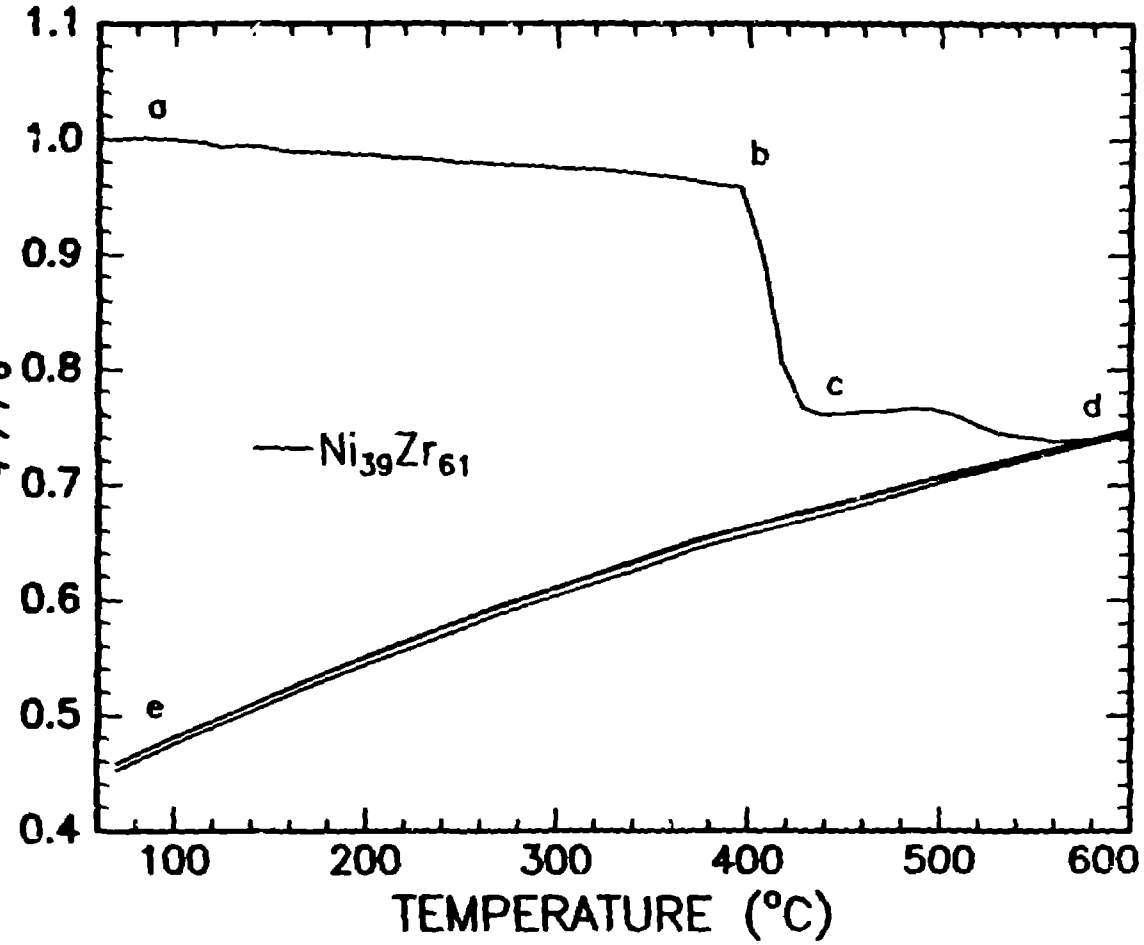
1.1
1.0
0.9
0.8
0.7
0.6
0.5
0.4
$\Delta\rho/\rho_o$
a
b
c
d
e
$Ni_{39}Zr_{61}$
100
200
300
400
500
600
TEMPERATURE (°C)

4.6.3

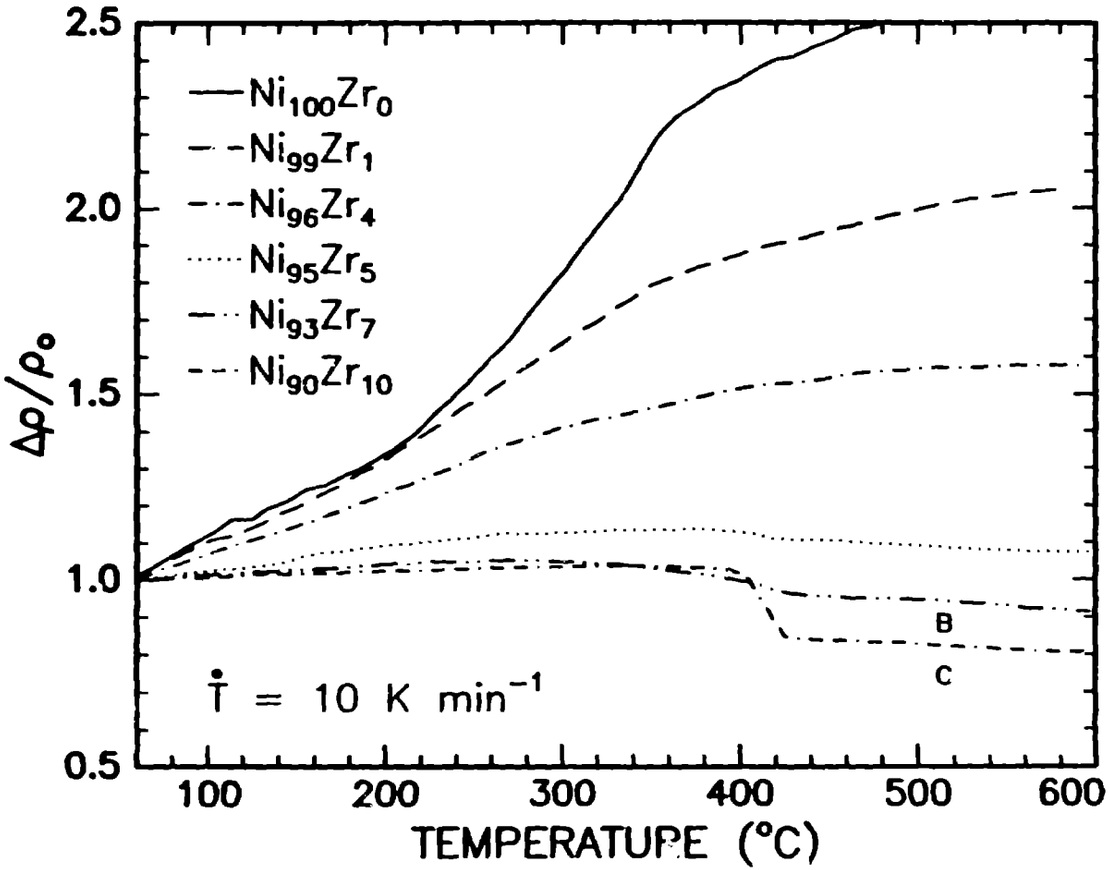
2.5
2.0
1.5
1.0
0.5
Δρ/ρ₀
Ni100Zr0
Ni99Zr1
Ni96Zr4
Ni95Zr5
Ni93Zr7
Ni90Zr10
Ṫ = 10 K min⁻¹
B
C
100
200
300
400
500
600
TEMPERATURE (°C)

Fig. 5

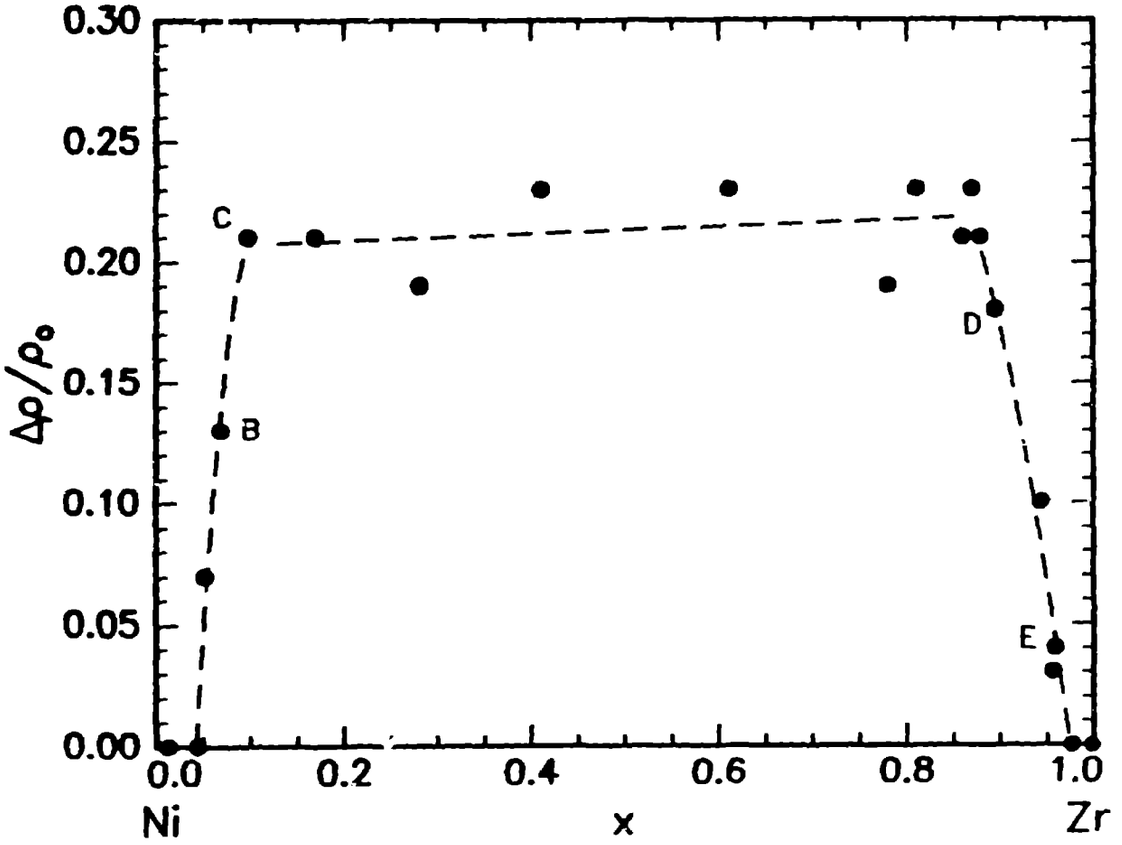

Fig. 6